Deagglomeration of DNA nanomedicine carriers using controlled ultrasonication

Beth A. Hinchliffe [a], Piers Turner [a,1], David J. H. Cant [a], Emiliana De Santis [a], Purnank Aggarwal [a], Rob Harris [b], David Templeton [b], Alex G. Shard [a], Mark Hodnett [a], Caterina Minelli [a,*]

[a] *National Physical Laboratory, Hampton Road, Teddington SW11 0LW, UK*
[b] *N4 Pharma, Weston House, Bradgate Park View, Chellaston DE73 5UJ, UK*

ABSTRACT

Control over the agglomeration state of manufactured particle systems for drug and oligonucleotide intracellular delivery is paramount to ensure reproducible and scalable therapeutic efficacy. Ultrasonication is a well-established mechanism for the deagglomeration of bulk powders in dispersion. Its use in manufacturing requires strict control of the uniformity and reproducibility of the cavitation field within the sample volume to minimise within-batch and batch-to-batch variability. In this work, we demonstrate the use of a reference cavitating vessel which provides stable and reproducible cavitation fields over litre-scale volumes to assist the controlled deagglomeration of a novel non-viral particle-based plasmid delivery system. The system is the Nuvec delivery platform, comprising polyethylenimine-coated spiky silica particles with diameters of $\sim$ 200 nm. We evaluated the use of controlled cavitation at different input powers and stages of preparation, for example before and after plasmid loading. Plasmid loading was confirmed by X-ray photoelectron spectroscopy and gel electrophoresis. The latter was also used to assess plasmid integrity and the ability of the particles to protect plasmid from potential degradation caused by the deagglomeration process. We show the utility of laser diffraction and differential centrifugal sedimentation in quantifying the efficacy of product de-agglomeration in the microscale and nanoscale size range respectively. Transmission electron microscopy was used to assess potential damages to the silica particle structure due to the sonication process.

1. Introduction

Recent advances in gene therapeutics and vaccine technologies have highlighted the importance of effective platforms to deliver oligonucleotides into cells. The use of particle-based systems as delivery vehicles have shown potential for protecting these fragile biopolymers, while at the same time enabling their delivery to the targeted site. Proposed particle platforms for the delivery of oligonucleotides [1–3] include protein constructs such as virus-based and virus-like particles, polymer particles [4–7], lipid-based particles such as liposomes and lipid-based nanoparticles [8,9] and inorganic particles. The most common inorganic carriers under development include silica nanoparticles [10–12], gold nanoparticles [13] and magnetic nanoparticles [14], but carbon nanotubes, graphene and quantum dots have also been proposed

[15–17]. Inorganic particles have the advantage over organic materials that they are more stable. Furthermore, the functionalisation or coating of their surfaces to generate a positive charge provides a relatively straightforward strategy for binding the negatively charged oligonucleotides. As an alternative, engineered stimuli-responsive linkers can also be used to conjugate the oligonucleotides onto the surface of the inorganic particles. As for any other complex nanomedicine, inorganic delivery vehicles need to be assessed for particle fate, potential toxicity and immunoresponse on a case-by-case basis.

The synthesis and functionalisation of inorganic nanoparticles is generally well established and experimental parameters can be fine-tuned to control the materials' properties. Upscaled manufacturing of inorganic nanoparticles for nanomedicine applications imposes some stricter control over the quality of the products. In particular,

uncontrolled particle agglomeration may prevent particles from reaching the targeted intracellular sites [18], as well as contribute to irreproducibility in product performance. Agglomeration is typically enhanced when the particles' surfaces are loaded, for example, with the plasmid cargo or other molecular moieties. This is due to the increased routes for interaction between particles, for example through van der Waals, hydrogen bonding and hydrophobic types of molecular interactions. It is therefore paramount to establish scalable de-agglomeration procedures that are effective and reproducible, but at the same time do not cause damage to the particles or the oligomeric cargo.

Ultrasound sonication is a well-established mechanism for the deagglomeration of particle materials in dispersion. Its exploitation at any manufacturing scale requires strict control of the uniformity of its cavitation field over the sample volume to minimise within-batch and batch-to-batch variability. At the National Physical Laboratory, we developed a multi-frequency reference cavitating vessel producing stable and reproducible cavitation fields and demonstrated its use for the sonication-assisted liquid phase exfoliation of graphene [19]. In this work, we applied similar processing techniques to assist the deagglomeration of novel engineered silica particles with a consistent, repeatable and measurable dose of acoustic cavitation. The particles are part of the Nuvec® platform (N4 Pharma, Chellaston, UK), which is a non-viral adjuvant delivery system for vaccines and cancer treatments. The product consists of mesoporous silica nanoparticles with a novel spiked structure and enhanced surface adhesion for oligomers [20,21] and has the potential to be used to deliver oligomers including plasmid DNA, mRNA or SiRNA to tumours. The peculiar structure of the particles appears to effectively protect oligomers from degradation by nuclease [18,22,23] and trials in mice demonstrated a high antibody response in vivo when DNA was delivered into cells using this platform [24]. The Nuvec particle platform can be manufactured at large scale and a number of strategies have been investigated to minimise uncontrolled agglomeration. We evaluated here the performance of controlled cavitation using different powers and at different stages of preparation, for example before and after the loading of the particles with plasmid. We assessed the efficacy of product de-agglomeration by using the methods

for particle analysis of laser diffraction (LD) and differential centrifugal sedimentation (DCS). We assessed potential damages to the silica particle structure by transmission electron microscopy (TEM). Furthermore, we assessed plasmid loading using X-ray photoelectron spectroscopy (XPS) and potential damages by circular dichroism (DC) and gel electrophoresis.

2. Materials and methods

Nuvec (N4 Pharma, Chellaston, UK) consists of spiky silica particles coated with polyethylenimine (PEI) with total diameter of approximately 200 nm (referred to as "coated silica particles" in the text). For this study, the same silica particles without PEI coating were also provided (bare silica particles), and Nuvec particles loaded with plasmid pcDNA-OVA (University of Queensland, St Lucia, Australia) were prepared (plasmid-loaded silica particles). To prepare samples for sonication, 1 mL of ultrapure water (resistivity 18.2 MΩ-cm) was added to a 25 mg aliquot of coated or bare silica particles and pipetted vigorously to mix. A further 4 mL of ultrapure water was added to bring the total volume to 5 mL, with a concentration of 5 mg/mL. The samples were then subject to controlled cavitation processing. For plasmid-loaded silica particles, 60 μL of a 10 mg/mL pcDNA-OVA dispersion were added to 2.5 mL of ultrapure water and mixed with equal part of 10 mg/mL Nuvec according to one of the three procedures shown in Fig. 1. At each stage of mixing, the dispersions were pipetted vigorously. The resulting ratio of plasmid to coated silica particles was approximately 1:40 (w/w) for all procedures.

A 17 L reference cavitating vessel was used for controlled sonication (Fig. S1 of the SI) [25]. This novel sonoreactor can produce intense cavitation fields that have a well-defined acoustic field distribution, are reproducible and stable during long periods of time [26]. The vessel used here consisted of 21 planar transducers, located in three rows of seven sources, positioned evenly about the cylindrical vessel periphery. In previous work, it was shown that with suitable control measures, sonicated samples increased in temperature by only 3 °C over four hours of intense sonication [19]. Acoustic cavitation is the stimulated expansion and collapse of microbubbles in response to an applied acoustic
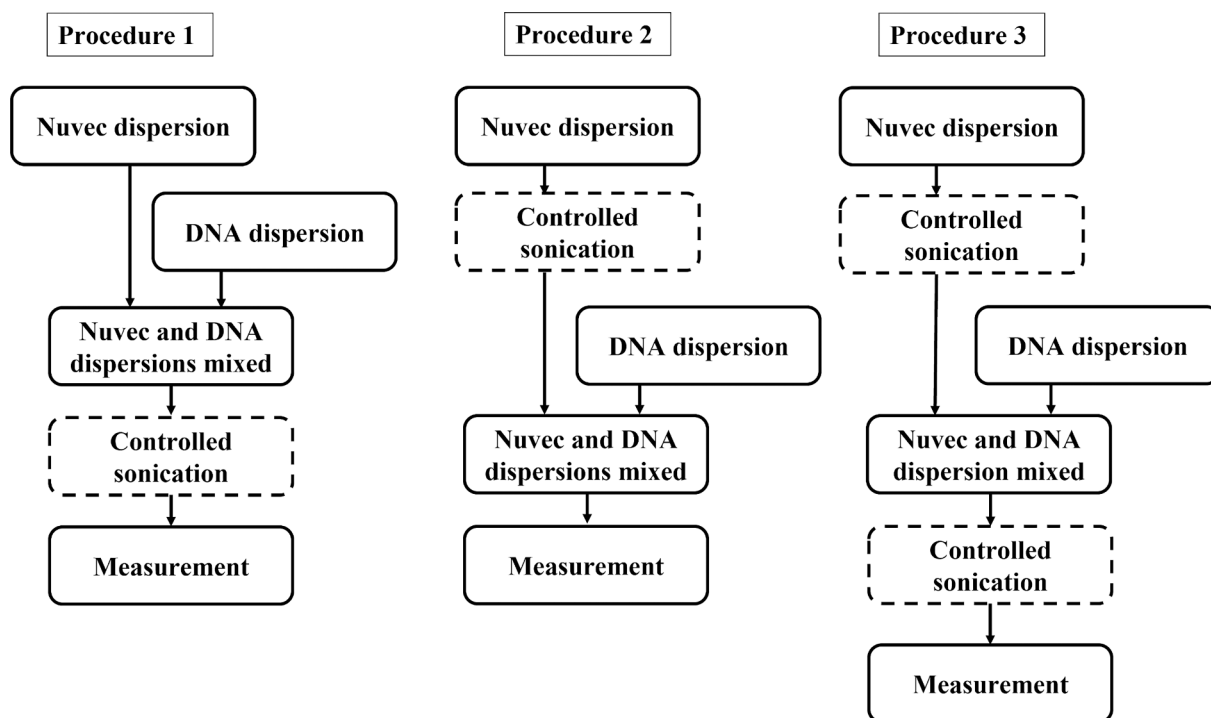

Fig. 1. Procedures investigated for the loading of Nuvec particles with plasmid pcDNA-OVA.

field. At low acoustic power densities, cavitating bubbles have long lifetimes and are referred to as non-inertial or stable cavitation, whereas at higher acoustic power densities cavitation bubbles can undergo violent and chaotic collapse; this is known as inertial cavitation. Inertial cavitation can be characterised by broadband acoustic noise, which can be measured using a broadband sensor [27]. Although the vessel is capable of multi-frequency operation [26], in this study, it was driven at a single frequency of 21.09 kHz using the signal generator of a PicoScope 5242B USB Oscilloscope (Pico Technology, St Neots, UK) via an E&I 1040L high-power radiofrequency amplifier (Electronics & Innovation ltd, Rochester, NY, USA), using a pre-amp voltage range of 90 mV_{RMS} (15 W) to 200 mV_{RMS} (100 W). In practice, this single-frequency operation meant that 7 of the 21 available transducers were energised, corresponding to the upper row of the vessel sources. All samples were decanted into 5 mL cylindrical Nalgene^{TM} low density polyethylene containers, and in turn, these were then located at the centre of the vessel for sonication, where cavitation is of high intensity, due to geometrical focal gain. The cavitation power in the liquid, arising from the sonication, P_{cav}, was determined according to Equation (1) [19]:

$$P_{cav} = \int_{f_1}^{f_2} V_{cav}^2(f) df \tag{1}$$

where $V_{cav}(f)$ are the frequency-dependent sensor voltages determined from the frequency-domain cavitation spectra and f_1 and f_2 are 1.5 MHz and 2.5 MHz respectively. The limits of integration were chosen to provide a measure of cavitation power which was minimally affected by environmental electrical noise in the system, and which was appropriate for the response bandwidth of the detector [19]. Representative spectra can be found in the supplementary information. The average cavitation power was calculated through experimental repeats. This approach demonstrated the highly non-linear nature of acoustic cavitation: the acoustic pressure field generated at 21.09 kHz gives rise to cavitation events which generate acoustic emissions at frequencies in the MHz region. The inertial cavitation dose is the product of the average P_{cav} value, which is measured every 2 s during a particular sonication, and the corresponding total duration, τ of the sonication protocol (e.g. from 300 s to 1800 s, as detailed). This 'dose' concept is described previously [28], and is used here as it allows meaningful comparison of the effects of different sonication regimes.

For the measurement of the size distributions, a loaded sample prepared according to procedure 3, showed good stability more than 90 min after the initial preparation. All other samples were transferred to the DCS and LD instruments well within 15 mins of the end of the sonication..

XPS measurements were performed with an Axis Ultra XPS instrument (Kratos, Manchester, UK), with a monochromated Al Kα X-ray source (photon energy 1486.6 eV). Survey spectra were obtained from the samples at a pass energy of 160 eV, and higher resolution spectra for specific elements were acquired at a pass energy of 20 eV. Samples for XPS analysis were dispersed in ultrapure water, dropwise deposited on a clean gold-coated substrate and dried under vacuum. Deposition was repeated in order to obtain a uniform thick deposit. Plasmid-loaded silica particles were prepared for XPS analysis according to two different protocols. For one sample, the coated silica particles were mixed with the plasmid according to procedure 2 and directly deposited onto the substrate. For the second sample, the dispersion was prepared according to procedure 2, but the resulting dispersion was subjected to three cycles of centrifugation and redispersion in ultrapure water to remove potentially unbound plasmid from solution. For each deposited sample, three non-overlapping regions of the deposit were measured by XPS, and the average results across these areas were reported. XPS spectra consist of peaks corresponding to electron core levels within the sample: when exposed to an incident X-ray beam, electrons are emitted from these core levels according to the photoelectric effect, and their energy and intensity are measured. This allows identification of

elements and chemical states at the surface of the sample based on measured electron energies, and quantification of these based on the measured intensity. XPS data were analysed using CasaXPS software, version 2.3.22. The results from the XPS measurements are reported as homogeneous-equivalent atomic concentrations in atomic fractions expressed as a percentage (at%). Due to the high surface sensitivity of XPS, materials closer to the surface will have a higher at% than the average concentration within the sampling depth, whereas the at% of buried materials will be reduced. The uncertainties in measured atomic concentrations are approximately 15 % for most elements and may be up to ∼ 20 % for elements present below 5 At%, or up to ∼ 100 % for elements close to the XPS detection limits.

LD measures the diffraction pattern generated by a particle sample when exposed to a monochromatic beam of light. The light intensity and diffraction angles are measured and used to infer a particle size distribution according to Mie theory [29]. The size distribution measured by LD is typically called a density or frequency distribution. The areas underneath a density distribution shall remain constant, independent of the transformation of the x-axis between a logarithmic and linear scale [30]. LD measurements were performed with a Mastersizer 3000 equipped with the Hydro SV dispersion unit (Malvern Panalytical, Malvern, UK) and software v.3.71. Two light sources were used in sequence: a Helium-Neon laser emitting red light (4 mW, wavelength of 632.8 nm) and a blue LED light source (10 mW, wavelength of 470 nm). The particle size distribution was calculated using a refractive index of 1.457 at 632.8 nm and 1.464 at 470 nm [31]. The refractive index of water was set at 1.33 for both wavelengths. A non-spherical approximation was used in the analysis, which is designed for particles that are irregular in shape or have a rough surface structure.[32] Ultra-pure water was used for the background measurements, and 0.3 mL of the processed coated silica particle suspension (5 mg/mL) was added for the sample measurements. Degassing the ultrapure water in a sonicating bath prior to analysis was used to reduce the occurrence of bubbles. The particle concentrations and speed of the stirring bar utilised in the measurement were optimised prior to the measurements. Uncertainties were determined as the standard deviation of five replicate measurements.

DCS measures the time it takes particles to sediment through a fluid of known density in a centrifugal field. While sedimenting, the particles separate based on their size and density. During their motion, the particles traverse a 405 nm diode laser beam which is placed close to the edge of the disc. The light extinction is measured as a function of the sedimentation time by a photodetector, which sits opposite the light source on the other side of the rotor. The diameter of the sphere having equivalent sedimentation time as the sample particle is measured according to Stokes' law and requires knowledge of the sample density, the diameter and density of a particle calibrant and the average density of the fluid. The light extinction-based size distribution of the sample is then converted to a volume-based size distribution by using Mie's theory and modelling the sample particles as perfect rigid spheres. DCS measurements were conducted with a CPS 24,000 Disk Centrifuge running version 11 of the software (CPS Instruments, Prairieville, USA). Prior to the measurements, a density gradient was built within the centrifuge disc, according to manufacturer instructions: the disc was filled with 14.4 mL of a sucrose (Fisher Scientific, Loughborough, UK) solution with a concentration gradient varied between 240 g/kg and 80 g/kg (average density of gradient between the particle injection and nominal detection point is 1.064 g/mL), topped with 0.5 mL of dodecane to prevent evaporation. The gradient was left to thermally equilibrate for 30 min prior to the analysis. All measurements were performed at rotational speed of 20,000 rpm and injection volume of 100 µL. Before each sample injection, the instrument was calibrated using polyvinylchloride (PVC) particles of nominal diameter of 263 nm and density of 1.39 g/cm^3 (CPS Instruments) [33].

For gel electrophoresis the samples loaded on the gel were divided into two groups, heparin (Sigma-Aldrich, St. Louis, USA) treated and

untreated. Heparin was used to disrupt electrostatic interactions between the pcDNA-OVA and the coated silica particles and promote migration of the plasmid through the gel, whilst coated silica particles were expected to be retained in the gel loading well, due to their size. 100 IU heparin was dissolved in nuclease-free water and incubated for 1hr at 37 °C with pcDNA-OVA (un-sonicated and sonicated) and, plasmid-loaded silica particles prepared according to Procedures 2 and 3 (Fig. 1). The working concentration of plasmid when in heparin was 15 ng/µL, assuming an initial concentration of pcDNA-OVA on the particles of 120 ng/µL. The samples were diluted in Gel Loading Dye, Purple, no SDS (New England Biolabs, Ipswich, USA) and nuclease-free water to give a final loading DNA concentration of 9.26 ng/µL for both heparin treated and untreated samples. Agarose (Fisher, Waltham, USA) was dissolved in tris acetate ethylenediaminetetraacetic acid (TAE, Fisher, Waltham, USA) by heating in a microwave to produce a 1.5 % w/v agarose gel. The DNA was selectively detected using a DNA-specific SYBR™ Safe DNA Gel Stain (Invitrogen, Waltham, USA). After the stain was mixed into the molten agarose gel according to manufacturer instructions, the gel was poured in a gel tray and allowed to set at room temperature for 20 min. The gel box was powered by a BioRad Power Pac 200 which supplied 100 V and was run for 1.5 h in 1x TAE buffer. A 1 kb DNA ladder (New England Biolabs, Ipswich, USA) was loaded onto the gel to be used as a reference to measure plasmid and plasmid fragments molecular weight.

Circular dichroism (CD) measures the differential absorption of left- and right-handed circularly polarised light as a function of the illumination radiation wavelength and provides information on the secondary structure of chiral biomolecules in their region of absorption. Due to the absorbance-based nature of the technique, sample transparency is a prerequisite for CD measurements. Particle-bound DNA particles were not suitable for CD analysis, due to significant opacity. Measurements were therefore performed on the pcDNA-OVA samples only. Spectra were recorded on a JASCO J-810 (JASCO, Great Dunmow, UK) spectropolarimeter fitted with a Peltier temperature controller. The measurements were taken in ellipticities in millidegrees (mdeg). The data was collected with a 1 nm step, 1 s collection time per step, and presented as the average of 4 scans. All measurements were recorded in a quartz cuvette with 0.05 cm pathlength. All spectra were background corrected.

Transmission electron microscopy (TEM) measures the transmission of an electron beam through a thin specimen, where image contrast is determined by differences in electron densities of the materials in the sample. TEM micrographs of coated silica particles were recorded using a Talos Arctica transmission electron microscope (Thermo Fisher Scientific, Waltham, USA) equipped with a Ceta camera (Thermo Fisher Scientific, Waltham, USA) and K3-Bioquantum camera and energy filter (Gatan Inc, Pleasanton, USA) and operated at 200 keV. The micrographs reported here were acquired using the Ceta camera at a magnification of 120 k× (8 px/nm) or 190 k× (13 px/nm). Droplets of solution (5 µL) were deposited on glow-discharged Cu grids (200 mesh) coated with formvar/carbon film (Agar Scientific ltd) and stained with uranyl acetate (aq. 2 %, w/v) for 20 s, before removing excess solvent by blotting using grade 1 filter paper (Whatman, Sheffield, UK).

3. Results

Analysis by XPS of the bare and coated silica particles revealed that there were no significant contaminants at the surface of the products (Fig. S2A and B of the Supporting Information (SI)). XPS homogeneous-equivalent elemental compositions are shown in Table 1. Analysis of the plasmid-loaded silica particles spectra in Fig. 2 demonstrated the presence of phosphorus with a P 2p binding energy position consistent with the phosphate environment. The presence of phosphate from the DNA backbone is expected if the plasmid is adsorbed to the surface of the particles. XPS analysis did not reveal any significant difference in phosphorus surface concentration before or after removal of unbound plasmid molecule from the dispersion through centrifugation. This result suggests that at the concentration of plasmid used there is minimal excess plasmid in the supernatant following the initial mixing of coated silica particles and plasmid. The surface concentration of plasmid inferred from the P 2p peak intensity is rather small compared to the surface concentration of PEI and we were unable to confirm the presence of plasmid using the N 1 s and C 1 s regions due to strong and overlapping intensity in these regions from PEI. However, it is notable that the nitrogen content of the surface increases by approximately 2 at%,

Table 1
XPS homogeneous-equivalent elemental compositions of bare, coated and plasmid-loaded silica particles in at%.

Element	oxygen	carbon	nitrogen	silicon	phosphorus
Bare silica particles	63.2	1.6	0.0	35.1	0.0
Nuvec	43.9	22.2	8.6	25.3	0.0
Plasmid-loaded Nuvec	39.7	28.4	10.8	20.8	0.4
Washed plasmid-loaded Nuvec	40.5	26.9	10.3	21.9	0.4
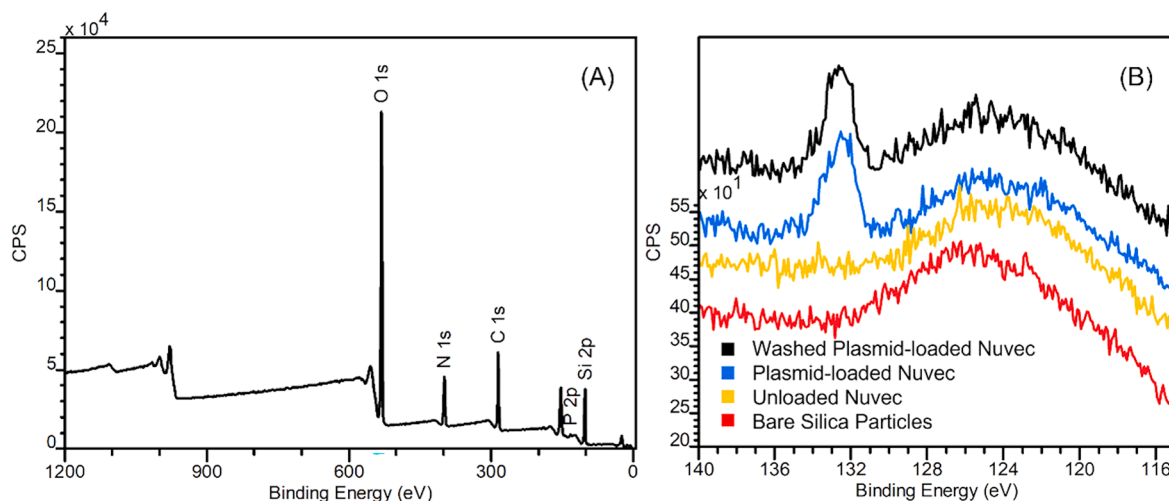
Fig. 2. (A) Representative XPS survey spectrum of the plasmid-loaded silica particles. (B) Representative XPS high resolution spectrum of the P 2p region of the plasmid-loaded silica particles (blue and black), bare silica particles (red) and PEI-coated silica particles (yellow). Data are scaled and offset for clarity. The peak at ~ 133 eV binding energy is typical of the phosphate environment. The structure in the background is due to energy loss from the Si 2p peak.

and this is similar to the increase expected if the phosphorus concentration was due to the plasmid. There are in fact approximately 3.75 nitrogen atoms to every phosphorus atom in DNA and the observed 0.4 at% of phosphorus suggests an additional 1.5 at% of nitrogen (Table 1).

LD was used to measure the particle size distributions of coated silica particles as a result of the cavitation processing under different conditions and determine the optimised dose for deagglomeration. Fig. 3 shows typical LD size distributions resulting from processing performed at different pre-amp voltages but for same 30 min duration (Fig. 3A) and same of 140 mV$_{RMS}$ voltage but for different durations (Fig. 3B), i.e. different cavitation doses. The distributions are characterised by a peak with modal diameter below 1 μm and additional peaks at larger diameters. Fig. 3A shows that after 30 min of processing, the intensity of the peaks at larger diameters decreases with increasing amplitude of the treatment, suggesting a decrease in the concentration of large agglomerates. Fig. 3B shows that for the same applied voltage, there is a decrease in the intensity of the peaks at larger diameters for longer treatments, again suggesting a more effective particle deagglomeration for longer durations of the processing.

DCS was used to measure the particle size distribution with high resolution, so to assess the effectiveness of the deagglomeration process for the particle populations below 1 μm. Fig. 3C shows the samples subject to 30 min of processing at different amplitudes, while Fig. 3D shows the samples subject to different durations of processing performed at the same amplitude of 140 mV$_{RMS}$. The measured size distributions were characterised by a peak at ~ 130 nm, followed by peaks at ~ 155 nm and ~ 172 nm, as well as a broader peak at larger size. It should be noted that these diameters were measured by assuming a density for the particles of 2 g/cm^3, i.e. the bulk density of silica, and assuming a spherical shape of the particles. We know that both these assumptions are untrue because silica particles exhibit a PEI coating and a spikey morphology. In this respect, the measured size distribution should be interpreted as that of perfect silica spheres having density of 2 g/cm^3 and equivalent time of sedimentation. The average particle density is expected to be lower than that of bulk silica due to the presence of the PEI coating, the Stokes' diameter of the particles is expected to be larger than 130 nm. However, it is difficult to provide an absolute measurement of the average particle diameter without a detailed particle model.

Nevertheless, the measured size distributions are useful to assess deagglomeration upon processing. The peak at 130 nm diameter shows the monodisperse coated silica particle population, while the populations at 155 nm and 172 nm show the dimeric and trimeric populations respectively, because in sedimentation the modal diameters of the dimer and trimer are approximately 1.2 and 1.3 times the primary particle diameter respectively [34]. The broader peak at larger modal diameter is likely to result from the convolution of the populations of higher order of agglomerates. Increasing the amplitude or the duration of the treatment does not appear to affect significantly the relative concentrations of these populations, although the peak of the monodisperse population is observed to increase in intensity. This increased intensity would reflect an increase in concentration of this population of particles [35].

Interestingly, a similar pattern in agglomeration is observed for the bare spikey silica particles before any PEI coating is applied. This is shown in Fig. S3 of the SI, where the representative size distributions of dispersions of the spikey particles before and after the addition of PEI coating as measured by DCS are shown. This result suggests that along with a narrowly distributed population of monodisperse particles, there are also some smaller populations of particles that are aggregated as a result of the synthesis of the silica particles, before the coating with PEI. It should be noted that both dispersions were subjected to controlled sonication under similar conditions before measurements. Successful application of the coating is consistent with the apparent shift towards lower sizes of the coated particles with respect to the bare silica particles. The presence of the coating causes a decrease in the average density of the particles and a consequent increase of their sedimentation time. However, because the size distributions are plotted assuming a density of 2 g/cm^3 for both samples instead of their real (unknown) density, the less dense material is shifted towards smaller diameters [36].

To compare the efficacy of the deagglomeration processes, the relative volume of the particle population with lower modal diameter according to LD measurements was computed and plotted against the square root of the cavitation dose. This is shown in Fig. 3E, where the relative volume of deagglomerate particles (i.e. the population with lower modal diameter) is seen to increase as function of the square root of the inertial cavitation. While initially the volume of deagglomerated particles appears to increase linearly with the square root of the inertial
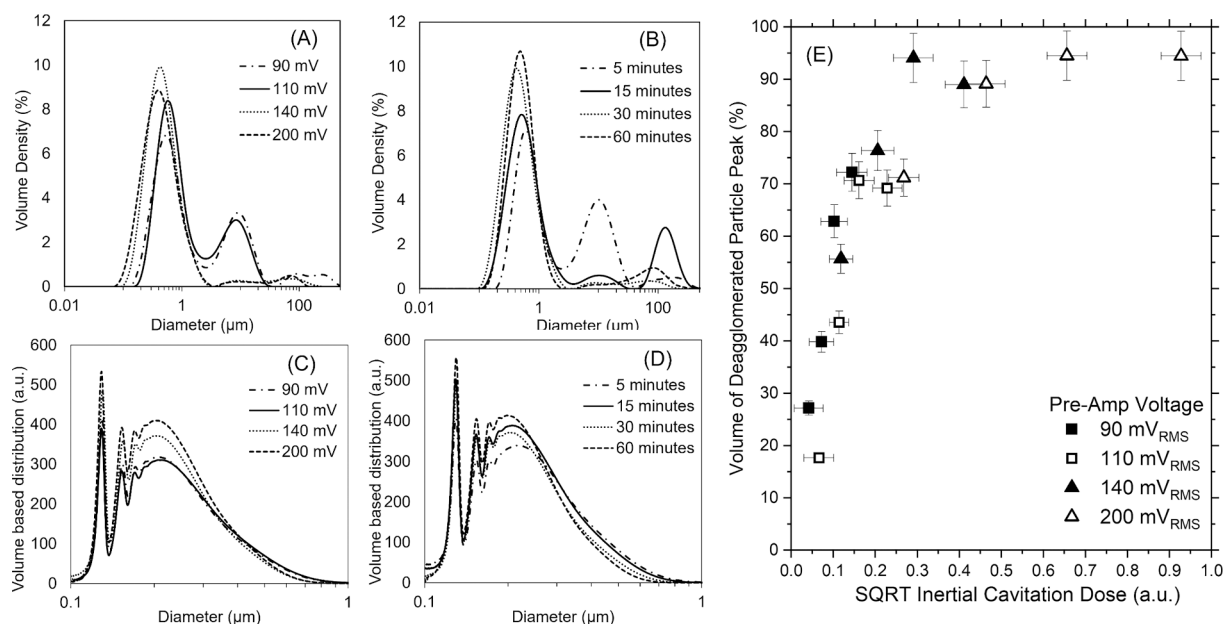
Fig. 3. Volume-based particle size distributions of the coated silica particle suspensions as measured by laser diffraction (A and B) and DCS (C and D). A and C show size distributions after 30 mins sonication at set pre-amp voltages. B and D show size distributions after a sonication at 140 mV$_{RMS}$ is applied for different time durations. DCS distributions plotted modelling the particles as spheres of density 2 g/cm^3. (E) The relative volume of deagglomerated particles with diameter below 4 μm according to LD measurements plotted against the square root (SQRT) of the inertial cavitation dose for sonicated Nuvec dispersions.

cavitation, this reaches a plateaux at 90 % of the inertial cavitation dose, suggesting the minimum sonication settings for optimal deagglomeration with the multi-frequency reference vessel is 140 mV$_{RMS}$ pre-amp voltage (42 W) for a duration of 30 min. This is therefore the condition that was selected for the deagglomeration of the particles later.

The next step consisted in evaluating the best conditions to ensure the deagglomeration of the plasmid-loaded silica particles and whether subjecting the plasmid to this processing could cause any damage to the plasmid. For this reason, we evaluated three different preparation protocols shown in Fig. 1. In procedure 1 and 2, the plasmid was added to the coated silica particles before and after controlled sonication respectively. In procedure 3 two cycles of controlled sonication were applied, before and after the addition of the plasmid. Procedure 1 was immediately excluded because the plasmid-particle complex resulted in a gel-like compound that could not be handled easily for further processing or measurements. Fig. 4A and B show the size distributions of the plasmid-loaded silica particles as measured by LD and DCS respectively. For comparison, the distribution of the partially deagglomerated coated silica particles before the addition of plasmid is also shown (dotted lines). As expected, procedure 3 appears more effective than procedure 2 in deagglomerating the particles. This is shown in Fig. 4A by a particle population with modal size below 100 μm appearing for samples processed according to procedure 3, but not procedure 2. LD measurements show large agglomerates in the size distribution for both samples compared to the unloaded PEI coated silica particle sample. Some level of agglomeration is also observed in the DCS size distributions, which are shown in Fig. 4B. The sample processed according to procedure 3 shows an agglomeration profile similar to the unloaded coated particles, but with a smaller population of monodisperse particles. For the sample processed according to procedure 2 we observe a peak with apparent mode below 100 nm that was not observed in previous measurements. It could be that this is representative of large and very low density plasmid agglomerates, possibly including silica particles but mostly comprising water, presumably in a gel. As previously discussed, the DCS distributions are plotted assuming a particle density of 2 g/cm^3, therefore particles with lower density and longer sedimentation times are shifted toward lower sizes.

We used TEM analysis to assess morphological changes between particles subjected to the selected processing conditions, for example due to the rupture of the silica spiked structures. Fig. 5 shows representative TEM micrographs of individual particles without (A and B) and with (C and D) negative staining and before (A and C) and after (B and D) loading with plasmid, using procedure 3, which delivered the highest total cavitation dose to the samples. Additional representative TEM images are shown in Figs. S4 and S5 of the SI for the particles prepared using procedure 2 and 3 respectively. The silica particles have inherent high electron density which allowed their visualisation without the use of negative staining as contrasting agent. TEM micrographs of sonicated particles showed that their spikey morphology, which is a critical feature for DNA binding, was not disrupted by the sonication treatment. Estimation of the particle size over a population of 100 particles by TEM resulted in average overall diameters of (200 ± 25) nm and (220 ± 30) nm for particles processed according to procedure 2 and 3 respectively. A diameter of 200 nm for single particles is consistent with size distributions measured by DCS (Fig. S3 in SI) and attributed to the coated silica monomeric particles. Small particle clusters were also observed by TEM (Figs. S4 and S5 of SI), which may explain the populations at larger modal diameters observed by DCS, for example with overall diameter around 500 nm.

Owing to its soft-nature, plasmid requires negative staining to increase contrast for visualisation by TEM. The electron micrographs of stained nanoparticles in Fig. 5C and D and Fig. S4B and S5B of the SI show an accumulation of staining between the spikes. However, because the coated silica particles also contain PEI that would also be highlighted by the staining, it is not possible to assess unambiguously the presence of plasmid pcDNA-OVA.

Gel electrophoresis of both the plasmid and the plasmid-loaded silica particles was performed to assess potential damage to the plasmid caused by the cavitation process. Heparin was utilised to disrupt the electrostatic interaction between the plasmid and the surface of the coated silica particles. Fig. S6 of the SI shows the outcome of the assay for samples both incubated in heparin and non. For the untreated plasmid, a strong band was observed at a mass larger than 1 kb, which is consistent with pcDNA-OVA having a size of 6.718 kb [37]. For the plasmid subject to cavitation, however, this band was replaced by a smear at lower molecular weights, indicating fragmentation and instability of the plasmid upon processing. Circular dichroism was employed to further test the stability of the plasmid and results are shown in Fig. S7 of the SI. CD spectra for the free plasmid alone showed similar spectral features for the sonicated plasmid and the untreated plasmids control. This may be interpreted as plasmid fragments retaining their secondary structure. In the case of the plasmid-loaded silica particles a band was observed at the same molecular weight as the untreated plasmid, suggesting that the plasmid was stable upon cavitation processing in presence of the particles. This hypothesis is corroborated by the fact that plasmid loaded particles prepared according to both Procedure 2 and 3 exhibit the same band patterns. Plasmid-loaded silica particles were sonicated according to procedure 3, however this was not the case for procedure 2. It should be noted, however, that for the experimental conditions utilised in this work, the dissociation of the plasmid from the coated silica particle was partial, with plasmid still detected within the loading well of the gel. The opacity of the sample prevented CD analysis
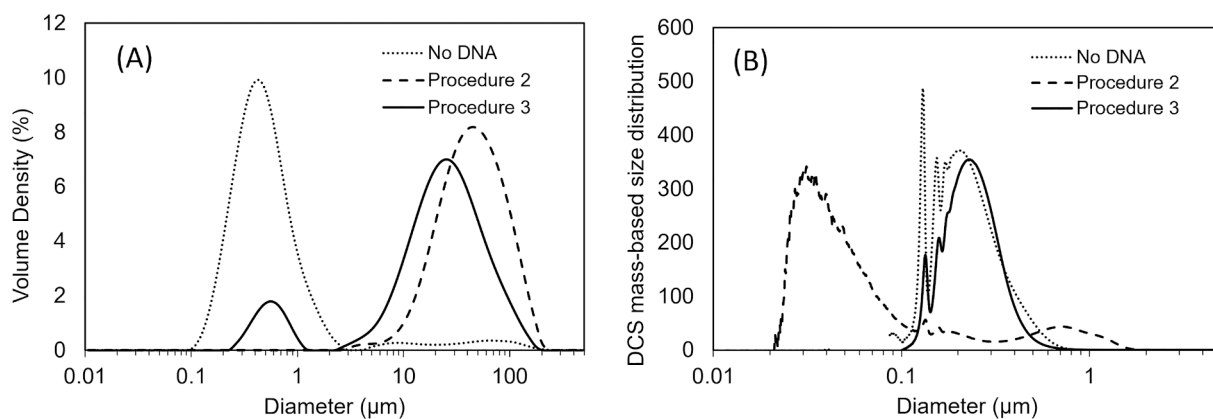

Fig. 4. Particle size distributions as measured by (A) LD and (B) DCS for partially deagglomerated coated silica particles (dotted line) and silica particles mixed with plasmid and subjected to procedure 2 (dashed line) and 3 (continuous line). DCS distributions plotted modelling the particles as spheres of density 2 g/cm^3. Controlled sonication at a pre-amp voltage of 140 mV$_{RMS}$ for 30 min.
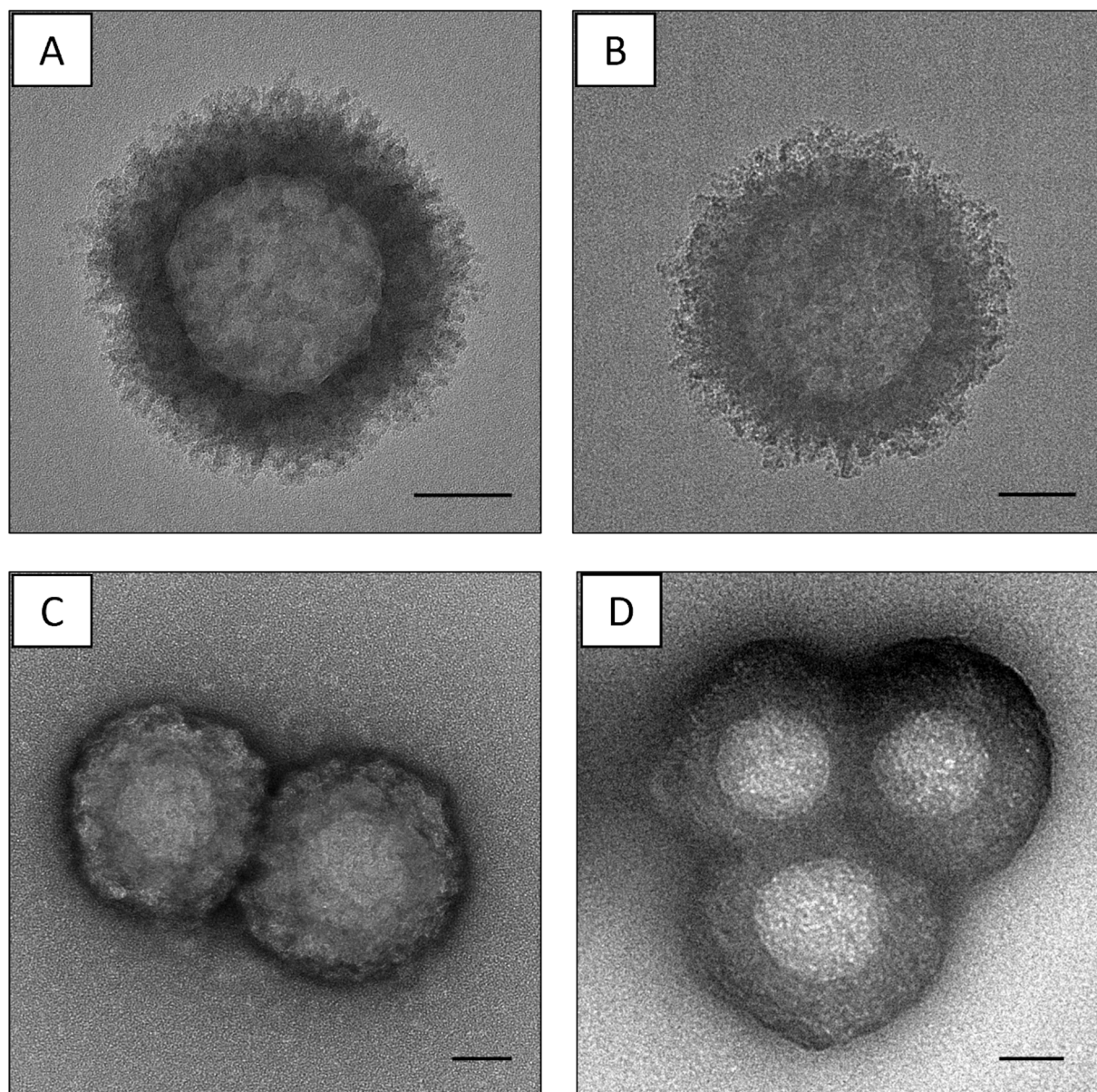
Fig. 5. Structural characterisation of Nuvec particles. Representative TEM micrographs of Nuvec particles prepared without (A,B) and with (C,D) negative stain imaged before (A, C) and after (B, D) loading with plasmid according to procedure 3. Scale bars are 50 nm.

of the plasmid-loaded silica particles. Although these results seem to point to the fact that its adsorption onto the surface of particles appears to protect the plasmid from fragmentation, cell transfection tests are required to exclude any damage to the plasmid bioactivity.

4. Discussion

Despite being widely available, ultrasound technology finds limited application in the manufacturing of pharmaceuticals. One limitation, even at bench scale, is the absence of objective, agreed measurement methods to characterise the generated excitation conditions. Off the shelf sonication devices vary significantly between manufacturers, and their available settings (which could be controls denoted in watts, watts per square cm, or amplitude in microns, or a dial with arbitrary numbered steps) are neither usefully comparable, nor suitable for providing a measurand on which to base a systematic effect assessment. Calibration techniques reported in the literature, examining the output of a sonication system, are often limited to calorimetry [38], and this provides no information on the acoustic field uniformity across the

volume hosting the sample. This increases the risk of irreproducible sample deagglomeration and damage to the processed materials.

The application of controlled sonication offers a number of advantages, as it allows a consistent application of intense cavitation fields resulting in reproducible deagglomeration of the particles. By using an in-line broadband sensor to monitor and optimise the cavitation field in real-time, this ensures a consistent cavitation dose is delivered for each sample. While sonic horns can deliver a comparable cavitation dose, they can be found to be less consistent/controllable, often due to variations in reported set-up conditions (e.g. the choice of liquid container and positioning), they can dramatically heat the sample, and can contaminate the sample through metal shedding during prolonged sonication. Achieving high levels of cavitation power through multitransducer vessels, particularly where geometrical focusing allows lower individual transducer operating levels, produces robust and repeatable processing capabilities, and can also generate cavitation over large liquid volumes. For industrial manufacturing, the sonication process needs to be applied and monitored consistently to large volume batches to enable upscaling of production, and this can be achieved

using multi-transducer sonication cells [19,26,39] of the type considered here, designed and configured for eventually achieving flow-based processing. Having control over the sonication dose by removing potential sources of set-up uncertainty means a higher reproducibility and consistency between processed batches can be attained.

Alternative strategies to particle deagglomeration involve the use of surfactants or other types of excipients. For highly engineered delivery systems such Nuvec, it is an important consideration to avoid the use of additives that may change the surface chemistry of the materials. The ability of Nuvec to load oligomers at the particles surface and the way they are released inside cells is thought to rely upon specific charge interactions between the delivery particles and the plasmid, as well as the cellular environment.

In this work we show the utility of controlled inertial cavitation to the deagglomeration of manufactured engineered silica nanoparticles designed for the intracellular delivery of macromolecules such as DNA plasmid. For the purposes of optimising the sonication dose, a matrix of inertial cavitation intensity and sonication duration, i.e. dose, was investigated. Fig. 2E shows that the ability of the process to induce deagglomeration initially increase linearly with the square root of inertial cavitation dose, before it levels off at high inertial cavitation doses. Based on this information the minimum dose to achieve optimum levels of deagglomeration was identified. The dependency of the outcome of materials processing on the square root of the inertial cavitation dose have been observed previously for different types of systems, for example the yield of graphene exfoliation upon sonication[19,40].

LD and DCS were used as qualitative methods to assess the effectiveness of the acoustic processing in deagglomerating the particles. The two methods provided complementary information on the size distribution of the particles, the former being useful to assess deagglomeration of large particle agglomerates upon processing, while the latter describing the monodisperse particle population as well as the low-coordination number agglomerates. The methods proved useful to identify changes in particle agglomeration upon processing. However, the measured size distributions could not deliver absolute size measurements due to the complex geometry and composition of the silica particles, which meant that the average particles' density and optical properties were unknown. This was further complicated by the presence of multiple populations of particles with different agglomerate coordination number and geometries. Both LD and DCS model all particle populations, including agglomerates, as perfect solid spheres with homogeneous materials properties, for example in terms of density and refractive index. This is because both methods, for example, rely on Mie theory to describe the interaction of light with particles, but the particle refractive index is not known with certainty due to the complex structure of the particles. TEM and XPS were utilised to confirm the geometrical and chemical composition of the particles. TEM imaging confirmed that the silica particles are not spherical, but instead have a complex surface structure of spikes, while the presence of the PEI coating was confirmed by XPS analysis. Despite this level of complexity, it was still possible to use the LD and DCS methods to observe relative changes to the samples upon different processing conditions. To enable a consistent comparison across samples, we used the values of density and refractive indexes of bulk silica at the wavelength of the light sources utilised by the instruments.

The addition of plasmid caused significant agglomeration of the silica particles. This is not unexpected given the size of the plasmid and its potential ability to bridge across particles. Furthermore, the adsorption of the plasmid at the particles' surfaces can cause a change in their surface charge, with consequent possible instabilities resulting in particle agglomerations. We compared the efficacy of different protocols in deagglomerating the particles. Procedures 2 and 3 were to some extent effective in reducing agglomeration, with procedure 3 resulting in a population of particles with modal diameter below 1 μm, similar to deagglomerated coated silica particles without plasmid. However, unlike procedure 2, procedure 3 also required sonication in presence of the

plasmid and an assessment of potential damages to the plasmid is required. Although a full assessment of the bioactivity of the plasmid would require cell transfection tests, we performed an initial investigation of the its integrity and that of the particle carriers. TEM investigation (Fig. 5) showed that the morphology of the Nuvec particles was not affected by the controlled sonication process. The spikey morphology of the silica particles, which is a key design feature to enable the successful loading of the plasmid and its intracellular delivery, was in fact retained upon sonication. Gel electrophoresis data appeared to suggest that the coated silica particles may play a role in preserving the structural integrity of the plasmid during sonication. Furthermore, CD results suggests that although the sonication process may cause plasmid fragmentation, these fragments still retained the ability to fold according to the plasmid secondary structure. In future, it will be important to complement this work with cell transfection studies aiming at quantifying the potential impact of particle processing on the bioactivity of the Nuvec delivery platform.

5. Conclusion

Deagglomeration of highly engineered silica particles with and without the presence of plasmid via controlled sonication was investigated. Controlled cavitation was delivered using a multi-transducer vessel and resulting size distributions of the particles were measured by LD and DCS. XPS and TEM were used to confirm the chemical and morphological structure of the Nuvec particles, as well as their successful loading with plasmid. By exploring a matrix of inertial cavitation doses, the minimum cavitation dose to maximise the deagglomeration of the particles was identified. Gel electrophoresis and CD spectroscopy were used to assess the effect of sonication on the structural integrity of the DNA plasmid bound to the coated silica particles. The results suggests that the particles may provide protection to the DNA plasmid from degradation.

Declaration of Competing Interest

The authors declare that they have no known competing financial interests or personal relationships that could have appeared to influence the work reported in this paper.

Data availability

Data will be made available on request.

Appendix A. Supplementary data

Supplementary data to this article can be found online at https://doi.org/10.1016/j.ultsonch.2022.106141.

References

[1] H. Zu, D. Gao, Non-viral Vectors in Gene Therapy: Recent Development, Challenges, and Prospects, AAPS J. 23 (2021) 78, https://doi.org/10.1208/s12248-021-00608-7.

[2] H. Yin, R.L. Kanasty, A.A. Eltoukhy, A.J. Vegas, J.R. Dorkin, D.G. Anderson, Non-viral vectors for gene-based therapy, Nat. Rev. Genet. 15 (2014) 541–555, https://doi.org/10.1038/nrg3763.

[3] A. El-Aneed, An overview of current delivery systems in cancer gene therapy, J. Control. Release 94 (2004) 1–14, https://doi.org/10.1016/j.jconrel.2003.09.013.

[4] D.W. Pack, A.S. Hoffman, S. Pun, P.S. Stayton, Design and development of polymers for gene delivery, Nat. Rev. Drug Discov. 4 (2005) 581–593, https://doi.org/10.1038/nrd1775.

[5] K. Miyata, N. Nishiyama, K. Kataoka, Rational design of smart supramolecular assemblies for gene delivery: chemical challenges in the creation of artificial viruses, Chem. Soc. Rev. 41 (2012) 2562–2574, https://doi.org/10.1039/C1CS15258K.

[6] N. Nishiyama, K. Kataoka, Current state, achievements, and future prospects of polymeric micelles as nanocarriers for drug and gene delivery, Pharmacol. Ther. 112 (2006) 630–648, https://doi.org/10.1016/j.pharmthera.2006.05.006.

[7] A.O. Abbas, M.D. Donovan, A.K. Salem, Formulating Poly(Lactide-Co-Glycolide) Particles for Plasmid DNA Delivery, J. Pharma. Sci. 97 (2008) 2448–2461, https://doi.org/10.1002/jps.21215.

[8] L. Taina-González, M. de la Fuente, The Potential of Nanomedicine to Unlock the Limitless Applications of mRNA, Pharmaceutics 14 (2022) 460.

[9] T.M. Allen, P.R. Cullis, Liposomal drug delivery systems: from concept to clinical applications, Adv. Drug. Deliv. Rev. 65 (2013) 36–48, https://doi.org/10.1016/j.addr.2012.09.037.

[10] I. Roy, T.Y. Ohulchanskyy, D.J. Bharali, H.E. Pudavar, R.A. Mistretta, N. Kaur, P.N. Prasad, Optical tracking of organically modified silica nanoparticles as DNA carriers: A nonviral, nanomedicine approach for gene delivery, Proc. National Acad. Sci. 102 (2005) 279–284, https://doi.org/10.1073/pnas.0408039101.

[11] C. Kneuer, M. Sameti, E.G. Haltner, T. Schiestel, H. Schirra, H. Schmidt, C.-M. Lehr, Silica nanoparticles modified with aminosilanes as carriers for plasmid DNA, Int. J. Pharm. 196 (2000) 257–261, https://doi.org/10.1016/S0378-5173(99)00435-4.

[12] M.V. Zyuzin, D. Zhu, W.J. Parak, N. Feliu, A. Escudero, Development of Silica-Based Biodegradable Submicrometric Carriers and Investigating Their Characteristics as in Vitro Delivery Vehicles, Int. J. Mol. Sci. 21 (2020) 7563.

[13] S. Rana, A. Bajaj, R. Mout, V.M. Rotello, Monolayer coated gold nanoparticles for delivery applications, Adv. Drug Deliv. Rev. 64 (2012) 200–216, https://doi.org/10.1016/j.addr.2011.08.006.

[14] J.R. Sosa-Acosta, C. Iriarte-Mesa, G.A. Ortega, A.M. Díaz-García, DNA–Iron Oxide Nanoparticles Conjugates: Functional Magnetic Nanoplatforms in Biomedical Applications, Top. Curr. Chem. 378 (2020) 13, https://doi.org/10.1007/s41061-019-0277-9.

[15] D. Pantarotto, R. Singh, D. McCarthy, M. Erhardt, J.-P. Briand, M. Prato, K. Kostarelos, A. Bianco, Functionalized Carbon Nanotubes for Plasmid DNA Gene Delivery, Angew. Chem. Int. Ed. 43 (2004) 5242–5246, https://doi.org/10.1002/anie.200460437.

[16] X.J. Loh, T.-C. Lee, Q. Dou, G.R. Deen, Utilising inorganic nanocarriers for gene delivery, Biomater. Sci. 4 (2016) 70–86, https://doi.org/10.1039/C5BM00277J.

[17] M. Vincent, I. de Lázaro, K. Kostarelos, Graphene materials as 2D non-viral gene transfer vector platforms, Gene Ther. 24 (2017) 123–132, https://doi.org/10.1038/gt.2016.79.

[18] D.M.F. Prazeres, G.A. Monteiro, Plasmid Biopharmaceuticals, Microbiol. Spectr. 2 (2014), https://doi.org/10.1128/microbiolspec.PLAS-0022-2014.

[19] P. Turner, M. Hodnett, R. Dorey, J.D. Carey, Controlled Sonication as a Route to in-situ Graphene Flake Size Control, Sci. Rep. 9 (2019) 8710, https://doi.org/10.1038/s41598-019-45059-5.

[20] H. Song, Y. Ahmad Nor, M. Yu, Y. Yang, J. Zhang, H. Zhang, C. Xu, N. Mitter, C. Yu, Silica Nanopollens Enhance Adhesion for Long-Term Bacterial Inhibition, J. Am. Chem. Soc. 138 (2016) 6455–6462, https://doi.org/10.1021/jacs.6b00243.

[21] H. Song, M. Yu, Y. Lu, Z. Gu, Y. Yang, M. Zhang, J. Fu, C. Yu, Plasmid DNA Delivery: Nanotopography Matters, J. Am. Chem. Soc. 139 (2017) 18247–18254, https://doi.org/10.1021/jacs.7b08974.

[22] S. Han, R.I. Mahato, Y.K. Sung, S.W. Kim, Development of biomaterials for gene therapy, Mol. Ther. 2 (2000) 302–317, https://doi.org/10.1006/mthe.2000.0142.

[23] D. Hobernik, M. Bros, DNA Vaccines—How Far From Clinical Use? Int. J. Mol. Sci. 19 (2018) 3605, https://doi.org/10.3390/ijms19113605.

[24] H. Song, Y. Yang, J. Tang, Z. Gu, Y. Wang, M. Zhang, C. Yu, DNA Vaccine Mediated by Rambutan-Like Mesoporous Silica Nanoparticles, Adv. Ther. 3 (2019) 1900154, https://doi.org/10.1002/adtp.201900154.

[25] M. Hodnett, M.J. Choi, Towards a reference ultrasonic cavitation vessel. Part 1: preliminary investigation of the acoustic field distribution in a 25 kHz cylindrical cell, Ultrason. Sonochem. 14 (2007) 29–40, https://doi.org/10.1016/j.ultsonch.2006.01.003.

[26] L. Wang, G. Memoli, M. Hodnett, I. Butterworth, D. Sarno, B. Zeqiri, Towards a reference cavitating vessel Part III—design and acoustic pressure characterization of a multi-frequency sonoreactor, Metrologia 52 (2015) 575–594, https://doi.org/10.1088/0026-1394/52/4/575.

[27] M. Hodnett, R. Chow, B. Zeqiri, High-frequency acoustic emissions generated by a 20 kHz sonochemical horn processor detected using a novel broadband acoustic sensor: a preliminary study, Ultrason. Sonochem. 11 (2004) 441–454, https://doi.org/10.1016/j.ultsonch.2003.09.002.

[28] W.-S. Chen, A.A. Brayman, T.J. Matula, L.A. Crum, Inertial cavitation dose and hemolysis produced in vitro with or without Optison®, Ultrasound Med. Biol. 29 (2003) 725–737, https://doi.org/10.1016/S0301-5629(03)00013-9.

[29] British Standards Institution. (2020) Particle size analysis — Laser diffraction methods (BS ISO 13320:2020) 10.3403/30333250.

[30] British Standards Institution. (1998) Representation of results of particle size analysis - Part 1: Graphical representation (BS ISO 9276-1) 10.3403/01507638.

[31] RefractiveIndex.INFO, Refractive Index Database https://refractiveindex.info/?shelf=main&book=SiO2&page=Malitson (04/04/2022).

[32] Malvern Instruments Ltd. (2017) Mastersizer 3000 user manual (MAN0474-08-EN-00).

[33] V. Kestens, V.A. Coleman, P.-J. De Temmerman, C. Minelli, H. Woehlecke, G. Roebben, Improved Metrological Traceability of Particle Size Values Measured with Line-Start Incremental Centrifugal Liquid Sedimentation, Langmuir 33 (2017) 8213–8224, https://doi.org/10.1021/acs.langmuir.7b01714.

[34] A.G. Shard, K. Sparnacci, A. Sikora, L. Wright, D. Bartczak, H. Goenaga-Infante, C. Minelli, Measuring the relative concentration of particle populations using differential centrifugal sedimentation, Anal. Methods 10 (2018) 2647–2657, https://doi.org/10.1039/c8ay00491a.

[35] C. Minelli, D. Bartczak, R. Peters, J. Rissler, A. Undas, A. Sikora, E. Sjöström, H. Goenaga-Infante, A.G. Shard, Sticky Measurement Problem: Number Concentration of Agglomerated Nanoparticles, Langmuir 35 (2019) 4927–4935, https://doi.org/10.1021/acs.langmuir.8b04209.

[36] N.C. Bell, C. Minelli, A.G. Shard, Quantitation of IgG protein adsorption to gold nanoparticles using particle size measurement, Anal. Methods 5 (2013) 4591–4601, https://doi.org/10.1039/C3AY40771C.

[37] S.S. Diebold, M. Cotten, N. Koch, M. Zenke, MHC class II presentation of endogenously expressed antigens by transfected dendritic cells, Gene Ther. 8 (2001) 487–493, https://doi.org/10.1038/sj.gt.3301433.

[38] Y. Son, M. Lim, J. Khim, L.-H. Kim, M. Ashokkumar, Comparison of calorimetric energy and cavitation energy for the removal of bisphenol-A: The effects of frequency and liquid height, Chem. Eng. J. 183 (2012) 39–45, https://doi.org/10.1016/j.cej.2011.12.016.

[39] D. Meroni, R. Djellabi, M. Ashokkumar, C.L. Bianchi, D.C. Boffito, Sonoprocessing: From Concepts to Large-Scale Reactors, Chem. Rev. 122 (2022) 3219–3258, https://doi.org/10.1021/acs.chemrev.1c00438.

[40] S. Marchesini, P. Turner, K.R. Paton, B.P. Reed, A.J. Pollard, Rapid monitoring of graphene exfoliation using NMR proton relaxation, Nanoscale 13 (2021) 14518–14524, https://doi.org/10.1039/D1NR03361A.